

## ESO-Based Backstepping Control of DC-DC Buck Converter Under Mismatched Load Disturbance

Akın Uslu<sup>1\*</sup> , Emrah Irmak<sup>1</sup> 

<sup>1</sup>Alanya Alaaddin Keykubat University, Rafet Kayış Faculty of Engineering, Department of Electrical and Electronics Engineering, Antalya, Turkey.

\*akin.uslu@alanya.edu.tr

### Abstract

The DC buck converter plays a critical role in supplying unfluctuated DC load voltage, however, which is exposed to various parametric uncertainties and disturbances operating under sensitive loads. This paper proposes a composite backstepping control strategy with an extended state observer (ESO) for the buck converter. Firstly, a backstepping control function is constructed to derive an inner current loop reference assuming load disturbance is known, which renders the global stability of the system. An ESO is designed to estimate the unmatched load current and collaborate with the backstepping controller to obtain disturbance attenuation. Quantitative selection of control and observer gains are provided under the highly nonlinear relationship of system dynamics. The rigorous stability of the proposed scheme is proved with an analysis of robustness. Finally, simulation results illustrate the comparative performance of the proposed control scheme against the disturbance caused by the load and uncertainties.

**Keywords:** Backstepping, Buck converter, Uncertainty, Observer.

## DA-DA Alçaltan Dönüştürücülerin Uyumsuz Bozucu Yük Altında GDG Tabanlı Geri Adım Kontrolü

### Özet

DC alçaltan dönüştürücüler dalgalanmayan DC yük gerilimi sağlamada kritik bir rol oynar, bununla birlikte hassas yükler altında çalışırken çeşitli parametrik belirsizliklere ve bozucu etkilere maruz kalmaktadır. Bu çalışmada alçaltan tip dönüştürücüler için genişletilmiş durum gözlemleyicisi (GDG) ile birlikte geri-adım kontrol stratejisini içeren tümlşik bir kontrol yapısı önerilmektedir. İlk olarak, sistemin genel kararlılığını sağlayan ve yük bozulmalarının bilindiği varsayılarak iç akım döngüsü referansı üretmek amacıyla bir geri-adımlama kontrol fonksiyonu oluşturulur. Daha sonra, eşleşmeyen yük akımını tahmin etmek ve bozulmayı azaltmak için geri adımlama denetleyicisi ile işbirliği yapmak üzere bir GDG tasarlanmıştır. Kontrol ve gözlemci kazançlarının seçimi, sistem dinamiklerinin doğrusal olmayan ilişkileri altında sağlanmıştır. Önerilen kontrol yapısının kesin kararlılığı, gürbzlük analizi ile birlikte sağlanmıştır. Son olarak, önerilen kontrol yöntemi için yükün ve belirsizliklerin neden olduğu bozulmalara karşı karşılaştırmalı performansını gösteren simülasyon sonuçları verilmiştir.

**Anahtar Kelimeler:** Geri-adım, Alçaltan dönüştürücü, Belirsizlik, Gözlemleyici.

## 1. INTRODUCTION

DC buck converter is one of the most popular power processing units to change the input/output voltage ratio of DC sources, which are widely applied in photovoltaic panels, renewable energy conversion, portable equipment, electric vehicles, HVDC, motor drives, and industrial processes [1-6].

The DC buck converter is modelled with unmodelled dynamics such as parametric uncertainties and disturbances. These unknown dynamics consist of time delay, parametric variation of passive elements, and unmodelled effects of no-ideal switching elements. Besides, input voltage and load variations are commonly encountered disturbances in the operation of DC buck converters. The main control objective in power circuits is to reach the desired voltage level on the output under source voltage variation and load resistor. To obtain satisfactory control performance, some of the linear approaches have been studied such as cascade proportional–integral (PI) control [7], and proportional-integral-derivative (PID) [8].

However, linear approaches are designed on the small-signal model of the converter around the desired operation points. Thus, only the local stability of the closed-loop system can be provided. When the DC-DC converter system is subjected to large fluctuations far away from the operating point, system stability may deteriorate. Furthermore, this leads to limited dynamic response of the closed-loop system.

To achieve a better dynamic response, various nonlinear control methods have been developed, such as robust control [9–11], adaptive control [12–14], sliding-mode control [15–17], intelligent control [18–20], and disturbance rejection control [21–23].

Predictive control has excellent dynamic response at the expense of relative computational load [24]. Except, predictive control has the disadvantage of adjusting the weighting factor. Although sliding mode control is robust to model uncertainties, it lacks the chattering phenomenon [25]. Repetitive control rejects periodic disturbance, but it has a relatively long internal time delay [26].

The above nonlinear approaches are evaluated from different perspectives according to advantages and sufferings, while they have two limitations in common. In one respect, they are insufficient to rigorously provide the large signal stability of the system. For another, it only focuses on uncertainty and disturbances, which take action on the same channels as the control law.

The large-signal stability of the system can be ensured with Lyapunov's direct method theory, which is designed based on a candidate Lyapunov function ( $V$ ). In the conventional approach for Lyapunov's, the control law and pseudo-variables are designed to ensure  $dV/dt < 0$  [27]. However, control law constructed merely has a single current control loop [28]. When extended for the DC-DC converter regulation, the output voltage is accompanied by steady-state error, which causes a slower dynamic response.

To solve this problem, [29] a virtual filter capacitor voltage is imported to the loop so that a two-loop control stability can be implemented. However, with this approach, the negative definiteness of  $dV/dt$  fails, which means the large-signal stability cannot be always guaranteed. It also makes load-current sensors mandatory for practical application.

Adaptive control is developed in [30], which has dual control loops to obtain satisfactory steady state and transient performance and also guarantee large-signal stability. Meanwhile, it obviates the use of load-current sensors. However, to construct the Lyapunov function systematically, backstepping control provides explicit rules that contribute to deriving the virtual reference states and control law within simplified design steps [31].

Most of the previous work only considers disturbances and uncertainties that take on the same channel as the control input which is called matched uncertainty. However, the output voltage of DC buck converters is also disturbed by the so-called unmatched variations like output current, which causes great difficulty for the robust controller design.

To address the mismatching problem, some variable structure schemes have been proposed such as sliding mode control (SMC), adaptive SMC [32], and SMC with integral action [33]. However, these studies

require definite disturbance bounds or first-time derivatives, which are hard to obtain due to the nonlinearity of DC buck converter systems.

Extended state observer (ESO) could achieve an estimation of the variations and disturbances without the knowledge of their boundary limits [34], which originally differs from the classical observers. It constitutes an integrator's chain to make the system canonical form and separate the actual plant from the nominal form plus a lumped disturbance. It lumps a wide range of uncertainties, including unmodeled dynamics, parametric variation, and external unknown disturbance. Thus, it provides a model-independent framework and a strong robustness and anti-disturbance ability.

Considering the limitations of the aforementioned approaches, this study proposes an ESO-based composite robust control approach to regulate buck converter voltage, whose main contribution is summarized as two points:

- The composite backstepping controller has a separate control structure, that could provide the large-signal stability of the system.
- To compensate for mismatched load current disturbance, ESO is designed to feedforward it to the backstepping controller, resulting in accurate tracking and rigid robustness.

## 2. SYSTEM DESCRIPTION AND MODELING

A basic pulse width modulated (PWM) DC buck converter is shown in Fig. 1. Where  $v_s$ ,  $i_L$ ,  $i_o$ ,  $v_o$  and  $u$  are input voltage, inductor current, load current, output voltage, and PWM input respectively. Mosfet (Q) and diode (D) are used as switching devices for the converter. The resistor of the load, inductor, and capacitor, which are the passive components of the circuit, are denoted by  $R$ ,  $L$ ,  $C$  respectively. The values of the components are given in Table 1.

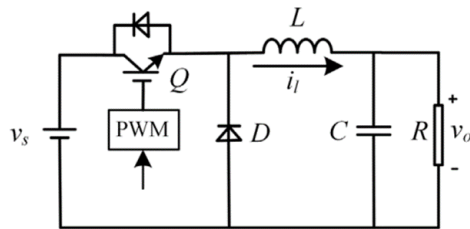


Figure 1. DC-DC Buck converter

Elements	Parameters	Values
Dc source voltage	$v_s$	20 V
Reference voltage	$v_r$	10 V
Filter inductor	$L$	4.3 mH
Filter capacitor	$C$	1000 $\mu$ F
Load resistor	$R$	100
Switching frequency	$f_s$	10 kHz

Ignoring the high-frequency dynamics of switching devices, the mean model of the DC buck dynamics is derived as follows:

$$L \frac{di_L}{dt} = uv_s - v_o \tag{1}$$

$$C \frac{dv_o}{dt} = i_L - \frac{v_o}{R} \tag{2}$$

The load resistance  $R$  is a major source of uncertainty and the variation in  $R$  causes the change of load current  $i_o$ , which is described as a disturbance for converter dynamics. For ease of representation and derivation, the following equivalent substitution is carried out, given by

$$x_1 = v_o, \quad x_2 = i_L, \quad \frac{v_o}{R} = i_o \tag{3}$$

where (1) can be rewritten as

$$C\dot{x}_1 = x_2 - i_o \tag{4}$$

$$L\dot{x}_2 = uv_s - x_1 \quad (5)$$

The control aim is to keep the load voltage  $v_o$  to a reference DC value. With the tuning of the PWM duty ratio  $\mu$ ,  $x_1$  is forced to track its reference  $x_1^*$ .

### 3. BACKSTEPPING CONTROLLER DESIGN

#### 3.1 Derivation of Inductor Current Reference

Load voltage error is expressed as

$$z_1 = x_1^* - x_1 \quad (6)$$

The Lyapunov candidate function for the load voltage error can be selected as

$$V_1 = \frac{1}{2}z_1^2 \quad (7)$$

Differentiating the Lyapunov function (7) along  $z_1$ , yields out that

$$\dot{V}_1 = z_1\dot{z}_1 \quad (8)$$

According to (4) and (6), the full derivation of (8) can be derived as

$$\dot{V}_1 = z_1(\dot{x}_1^* - \dot{x}_1) = z_1\left(\dot{x}_1^* - \frac{x_2 - I_o}{C}\right) \quad (9)$$

The pseudo-inductor current-reference  $x_1^*$  is chosen to ensure  $\dot{V}_1 < 0$ , given by

$$x_2^* = I_o + k_1 Cz_1 + C\dot{x}_1^* \quad (10)$$

where  $k_1$  is a positive constant, which is used for the controller parameter ( $k_1 > 0$ ).

If  $x_1$  is regulated to track  $x_1^*$ , (9) will be reformulated as

$$\dot{V}_1 = -k_1 z_1^2 \leq 0 \quad (11)$$

which becomes a negative semi-definite.

#### 3.2 Derivation of Control Law

The pseudo-tracking error for inductor current is expressed as

$$z_2 = x_2^* - x_2 \quad (12)$$

The second Lyapunov candidate function is composed of  $V_1$  and quadratic inductor current tracking error, defined as

$$V_2 = \frac{1}{2}z_1^2 + \frac{1}{2}z_2^2 \quad (13)$$

The time derivative of (13), is given as follows:

$$\dot{V}_2 = z_1\dot{z}_1 + z_2\dot{z}_2 \quad (14)$$

According to (9) and (12), a detailed derivation of (14) can be formulated as

$$\dot{V}_2 = z_1\left[\dot{x}_1^* - \frac{(x_2^* - z_2) - I_o}{C}\right] + z_2(\dot{x}_2^* - \dot{x}_2) \quad (15)$$

To guarantee  $\dot{V}_2 < 0$ , the control function can be chosen as

$$u = \frac{1}{V_s}\left(x_1 - L\dot{x}_2^* + \frac{L}{C}z_1 + k_2 z_2\right) \quad (16)$$

Where  $k_2$  is a positive constant, which is used for the controller parameter ( $k_2 > 0$ ). Substituting (16) into (15), the second Lyapunov function becomes negative semidefinite, given by

$$\dot{V}_2 = -k_1 z_1^2 - k_2 \frac{z_2^2}{L} \leq 0 \tag{17}$$

#### 4. DESIGN OF THE ESO TO ESTIMATE AND FEEDFORWARD THE LOAD CURRENTS FOR LOAD DISTURBANCE REJECTION

Eq. (10) shows that  $I_o$  is needed to generate a pseudo reference  $x_2^*$  on the aim of load disturbance rejection. Also load current sensor can be used to sense  $I_o$ , however, it increases the cost and deteriorates the system reliability. A better alternative, an ESO can be designed to observe  $I_o$  for control input [12]. With the help of the ESO observer, the proposed backstepping control law builds a nonlinear composite structure. Since  $I_o$  is unmeasurable in practice, an ESO for this type of control system can only be built using inductor current  $I_L$  as input and output  $v_o$  of the system assuming that  $I_o$  is differentiable w.r.t time and  $\dot{I}_o$  is bounded [22].

In the proposed control aim is to implement an ESO to estimate  $\hat{I}_o$ , so that disturbance effect of  $I_o$  can be rejected. To design the observer, output voltage dynamics in Eq. (1) is augmented with  $I_o$  and reformulated as in the following state space form:

$$\begin{cases} \dot{x} = Ax(t) + Bu_p(t) + Ef(t) \\ y_p(t) = C_p x(t) \end{cases} \tag{18}$$

where,

$$A_p = \begin{bmatrix} 0 & 1 \\ 0 & 0 \end{bmatrix} \quad B_p = \begin{bmatrix} 1 \\ C \end{bmatrix} \quad C_p = [1 \quad 0] \quad E = \begin{bmatrix} 0 \\ 1 \end{bmatrix}$$

$$y_p = V_o \quad u_p = I_L$$

The corresponding ESO can be configured as follows:

$$\begin{aligned} \dot{\hat{x}}(t) &= A_p \hat{x}(t) + B_p u_p(t) + L_p [y_p(t) - \hat{y}_p(t)] \\ &= (A_p - L_p C_p) \hat{x}(t) + B_p u_p(t) + L_p y_p(t) \\ \hat{y}_p(t) &= C_p \hat{x}(t) \end{aligned} \tag{19}$$

where  $\hat{x}(t) = [\hat{V}_o \quad \hat{I}_o]^T$  denotes the estimated state variable  $v_o$  and  $I_o$ , and  $L_p = [l_1 \quad l_2]^T$  is the observer gain matrix. The observation error  $x_e(t) = [x_{e1} \quad x_{e2}]^T$  of the ESO is

$$x_e = x(t) - \hat{x}(t) \tag{20}$$

and subtracting (19) from (18), we have

$$\begin{aligned} \dot{x}_e(t) &= Dx_e(t) + Ef(t) \\ D &= \begin{bmatrix} -l_1 & 1 \\ -l_2 & 0 \end{bmatrix}, E = \begin{bmatrix} 0 \\ 1 \end{bmatrix} \end{aligned} \tag{21}$$

Observer parameters are selected such that  $D$  is Hurwitz with desired eigenvalues. Bandwidth parametrization is a frequently used method for the observer gains [17],

$$s^2 + l_1 s + l_2 = (s + \omega_o)^2 \tag{22}$$

with  $\omega_o$  being the observer bandwidth. According to equation (20), observer parameters can be chosen as:

$$l_1 = 2\omega_o, l_2 = \omega_o^2 \tag{23}$$

A common rule of thumb is used to select the observer bandwidth as  $\omega_o = (2\sim 5)\omega_n$ , where  $\omega_n$  is controller natural frequency.

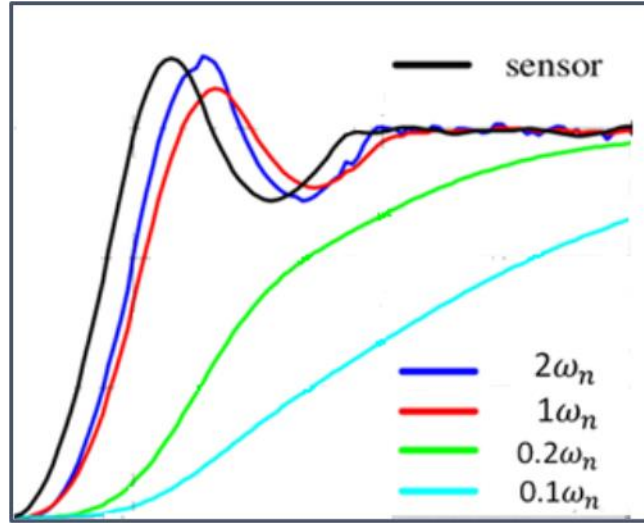


Figure 2. The tracking performance of the ESO as  $\omega_o$  varies

The tracking performance of ESO is shown in Fig. 2. It shows that choosing  $\omega_o$  needs a trade-off between controller bandwidth and disturbance sensitivity. When  $\omega_o = 2\omega_c$ , the estimated load current is almost the same as the sensor output, however, when  $\omega_o = 0.1\omega_c$ , it takes a very long time to reach the sensor value.

#### 4.1 Formation of ESO Based Backstepping Control

Then the estimated variables can be used to feedforward  $I_o$  to generate inductor current reference  $x_2^*$  as follows:

$$x_2^* = \hat{I}_o + k_1 C z_1 + C \dot{x}_1^* \tag{24}$$

The designed control law, including the disturbance rejection term and the backstepping controller, can be formulated as:

$$u = \frac{1}{V_s} \left[ x_1 + \frac{d}{dt} L(\hat{I}_o + C k_1 z_1) + \frac{L}{C} z_1 + k_2 z_2 \right] \tag{25}$$

It has two dual control loops, which are the outer voltage loop  $z_1$  and pseudo-inductor-current loop  $z_2$ . Voltage-loop control gain is  $k_1$  and current-loop control gain  $k_1$ . A block diagram of the buck converter controlled by the proposed control law is depicted in Fig.3.

PWM modulator compares the control signal  $u(t)$  with the triangle carrier wave to produce the switching gate signal mosfet. Inductor current  $i_l$  and output voltage  $v_o$  are measured by sensors. Besides, there is no need to measure load-current  $I_o$  due to estimation.

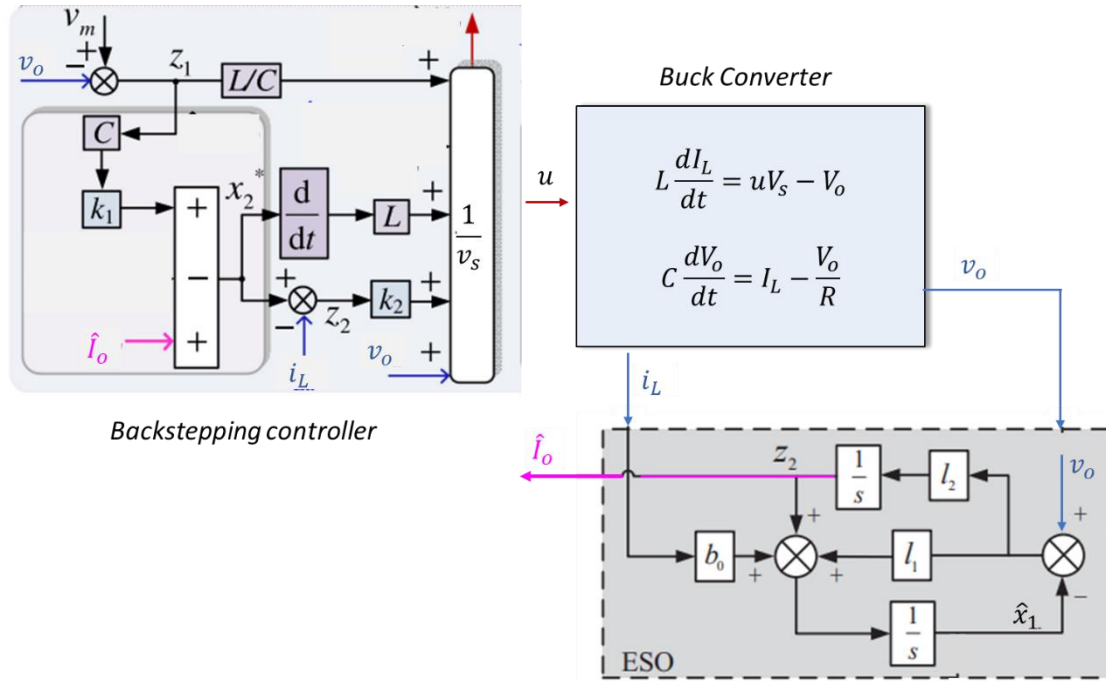


Figure 3. Blok diagram of ESO-based backstepping control for buck converter

To obtain quantitative controller gains, closed-loop error ( $z_1, z_2$ ) dynamics should be constituted. Substituting (16) to (4), it yields

$$C\dot{x}_1 = x_2^* - z_2 - I_o \tag{26}$$

The inductor current-loop reference (10) is substituted into (26), which gives out that

$$\dot{z}_1 = -k_1 z_1 + z_2/C \tag{27}$$

Similarly, the switching functions (16) is substituted to (5), which gives

$$\dot{z}_2 = -z_1/C - k_2 z_2/L \tag{28}$$

Error dynamics in (27), (28) can be written in compact form as

$$\dot{z}_c = Kz_c \tag{29}$$

where  $z_c = [z_1 \ z_2]^T$ , and

$$K = \begin{bmatrix} -k_1 & 1/C \\ -1/C & -k_2/L \end{bmatrix} \quad k_1 > 0, \quad k_2 > 0$$

The characteristic equation of matrix K is derived as

$$\det(sI - K) = s^2 + \left(k_1 + \frac{k_2}{L}\right)s + \frac{k_1 k_2}{L} + 1/C^2 \tag{30}$$

Equation (30), demonstrate that closed-loop error dynamics turned into a typical second-order system. So, the damping ratio ( $\xi$ ) and the natural frequency  $\omega_n$  can be used as main indicators for tuning the controller gains.

The parameters  $\xi$  and  $\omega_n$  directly indicate the steady-state and dynamic characteristics of the controlled system. The faster dynamic response can be obtained with larger  $\omega_n$ , which implies that state variables will be regulated to reach their references with less time. While larger  $\xi$  provides more damping for the system, which leads small overshoot while transient response.

Initially, (30) equates to the second-order characteristic equations, given by

$$\det(sI - K) = s^2 + (2\xi\omega_n)s + \omega_n^2 = 0 \tag{31}$$

Eq. (31) has two solutions for, described as  $s_{1,2}$ :

$$s_{1,2} = -\xi\omega_n \pm \omega_n\sqrt{\xi^2 - 1} \tag{32}$$

where  $\xi$  and  $\omega_n$  are derived as

$$\xi = \frac{CLk_1 + Ck_2}{2\sqrt{k_1k_2LC^2 - L^2}} \quad \omega_n = \sqrt{\frac{k_1k_2}{L} + \frac{1}{C^2}} \tag{33}$$

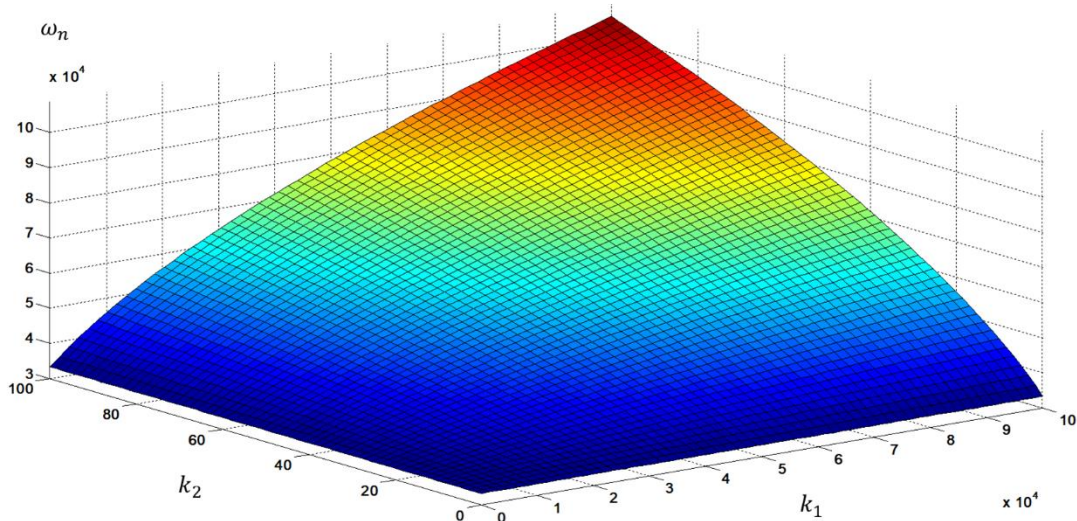


Figure 4. Natural frequency  $\omega_n$  as  $k_1$  and  $k_2$  increases

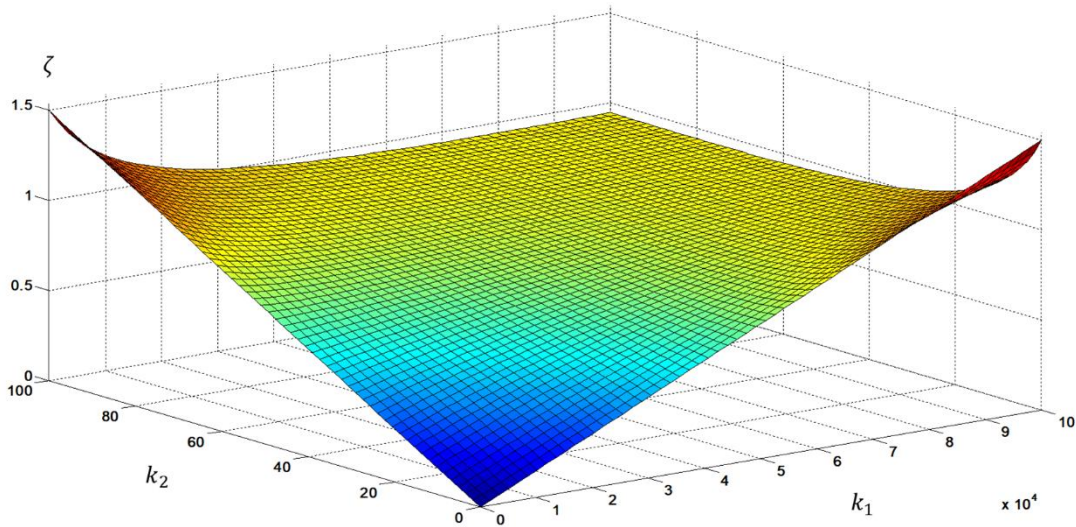


Figure 5. Damping ratio  $\xi$  as  $k_1$  and  $k_2$  increases

Fig. 4 and 5 depict the variation of  $\xi$  and  $\omega_n$  with the increase of  $k_1$  and  $k_2$  according to (33). It shows that  $\xi$  and  $\omega_n$  have a highly non-linear relationship with  $k_1$  and  $k_2$ . Although, control parameters  $k_1$  and  $k_2$  can be estimated from Fig. 4 and Fig. 5 it is hard to select  $\xi$  and  $\omega_n$  simultaneously. A better alternative is making a trade-off between settling time and overshoot during transients, where  $\xi$  is the fixed optimal damping ratio.

$$\xi = \frac{CLk_1 + Ck_2}{2\sqrt{k_1k_2LC^2 - L^2}} = \frac{\sqrt{2}}{2} = 0.707 \tag{34}$$

After mathematical transformation (34) can be rewritten as,

$$\frac{k_1^2}{(\sqrt{2}/C)^2} + \frac{k_2^2}{(\sqrt{2}L/C)^2} = 1 \tag{35}$$

Where  $k_1 > 0$  and  $k_2 > 0$ . Certainly, an equivalent parametric Eq. (36) can be expressed in the trigonometric aspect as,

$$\begin{aligned} k_1 &= \frac{\sqrt{2}}{C} \cos\theta & k_2 &= \frac{\sqrt{2}L}{C} \sin\theta \end{aligned} \quad \text{Where, } \theta \in [0, \pi/2] \tag{36}$$

Under this condition, the controller parameters ( $k_1, k_2$ ) can be determined optimally,

$$\begin{cases} k_1 = \sqrt{2}\cos\theta/C|_{\theta=\frac{\pi}{4}} = \frac{1}{C} \\ k_2 = \sqrt{2}L\sin\theta/C|_{\theta=\frac{\pi}{4}} = \frac{L}{C} \end{cases} \tag{37}$$

### 5. STABILITY

In this section, the stability of the ESO and the controlled system is analyzed. From (21), it can be seen that it is always possible to choose the observer constants  $l_1$  and  $l_2$  such that the eigenvalues of  $D$  can be placed in the left half plane. Thus, we can always define a positive definite matrix  $P$  such that.

$$D^T P + PD = -Q \tag{38}$$

for any given positive definite matrix  $Q$ . Assume that,  $\lambda_m$  is the smallest eigenvalue of  $Q$ . Defining a Lyapunov candidate

$$V_o = x_e^T P x_e \tag{39}$$

Then derivating along  $V_o$  along (21)

$$\begin{aligned} \dot{V}_o &= x_e^T (D^T P + PD)x_e + 2x_e^T P E \dot{f} \\ &\leq -x_e^T Q x_e + 2\|PE\| \|x_e\| \mu \\ &\leq -\lambda_m \|x_e\|^2 + 2\|PE\| \|x_e\| \mu \\ &\leq -\|x_e\| (\lambda_m \|x_e\| + 2\|PE\| \mu) \end{aligned} \tag{40}$$

It can be concluded from (40) that as time goes to infinity, the estimation error is ultimately bounded by

$$\|x_e\| \leq \lambda_1 \tag{41}$$

Where,

$$\lambda_1 = \frac{2\|PE\|}{\lambda_m} \tag{42}$$

Lyapunov function for the controller  $V_o$  is evaluated to prove the stability of the closed-loop system around (27), which is given by

$$V_c = z_c^T z_c \tag{43}$$

The time derivative of (43) is given by

$$\begin{aligned} \dot{V}_c &= \dot{z}_c^T z_c + z_c^T \dot{z}_c \\ &= z_c^T (K^T + K) z_c \\ &= z_c^T \begin{bmatrix} -2k_1 & 0 \\ 0 & -2k_2/L \end{bmatrix} z_c \end{aligned} \tag{44}$$

which proves that system stability is not affected by  $L, C$  if  $k_1, k_2 > 0$ .

### 6. SIMULATION RESULTS

In this section, the performance of the designed control law is simulated in Matlab in Fig 6. The conventional backstepping strategy, the ESO-based backstepping, and PI control methods are compared in terms of transient and steady-state response. The classical PI control unit is demonstrated by Eq. (45). For the ESO-backstepping, an extended state observer collaborates to estimate the unmatched uncertainties and load current. Control performance may vary concerning the parameters for many controllers. Therefore, to obtain a fair comparison between test controllers, the parameters of the three controllers have been tuned for their optimal response. The simulation aims to control the output voltage of the buck converter at reference in the condition of uncertainties and also to ensure the controllers track a desired reference voltage. The converter component and controller gains of the buck converter are summarized in Table 2.

$$u_{pi} = k_p z_1 + k_i \int z_1 \tag{45}$$

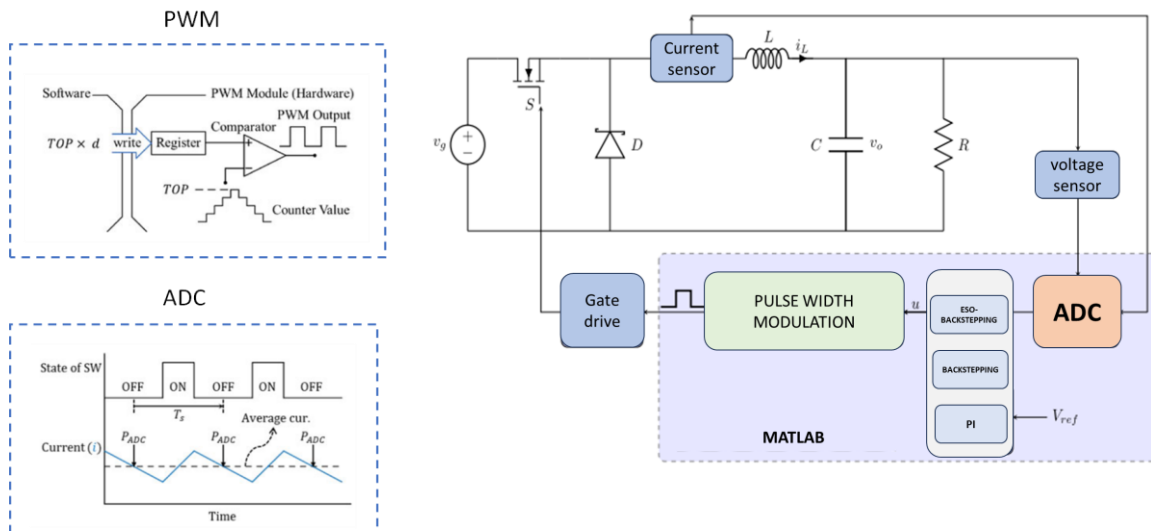


Figure 6. Block diagram of simulation setup

Table 2. Controller gains for buck converter

Control methods	Parameters
Backstepping	$k_1 = 10^3$ $k_2 = 4.7$
ESO	$l_1 = 5 \times 10^4$ $l_2 = 8 \times 10^6$
PI	$k_p = 10$ , $k_i = 5000$

### 6.1 Case 1: Variation of the Load

To evaluate the robustness against load variation, the resistance  $R$  is dropped from full load to half load at  $t = 3$  s, and the results are simulated in Fig. 7. while keeping nominal source voltage  $v_s$  at 24 V and  $V_{ref}$  at 10 V, It can be seen that both ESO-backstepping and backstepping achieve good robustness against the load changing compared to the backstepping, the ESO-backstepping dynamic performance is better with fast transient response and less overshoot. However, in the classical PI, a large steady tracking error prevents it from reaching the desired output voltage. In addition, the ESO-backstepping is observed superior disturbance reduction compared with the other schemes. Both the ESO-backstepping and backstepping achieve a true estimation of the unmatched uncertainties, but the ESO-backstepping response is faster than other schemes.

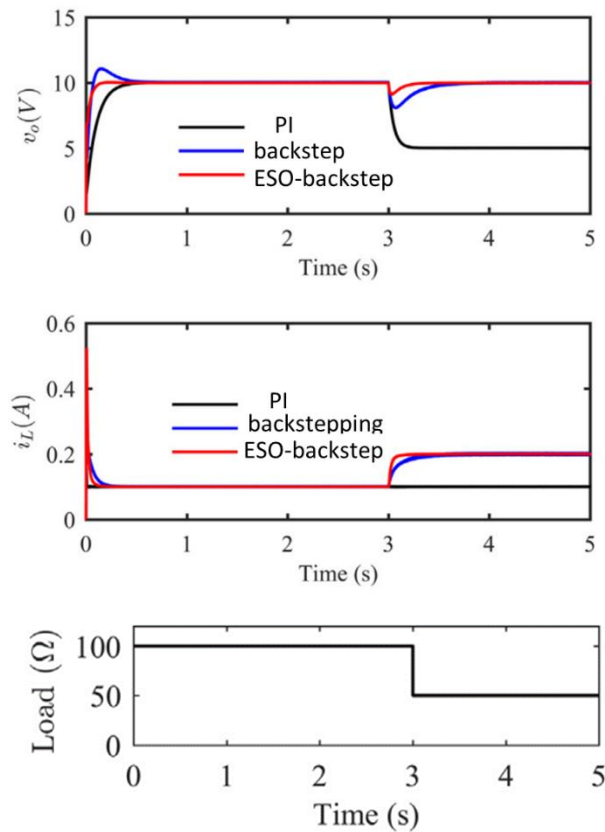


Figure 7. Buck converter with half load change

### 6.2 Case 2: Variation of Source Voltage

The input voltage  $v_s$  is changed in a step and drop fashion from 20-24-16 V while keeping load resistance as nominal and setting  $V_{ref}$  voltage at 10 V. Keeping the controller configuration constant, simulated controller results are shown in Fig. 8. Until  $t = 4$  s, it is observed that the backstepping and PI reach the reference output voltage, which means the robustness against to the matched uncertainties is verified. However, at  $t = 4$  s, the output voltage of backstepping and PI have a large steady-state error because the

control gains of the two controllers are insufficient to prevent the magnitude of disturbance. In the condition of input voltage variation, the ESO-backstepping achieved a 10 V output voltage again with a short-term transient.

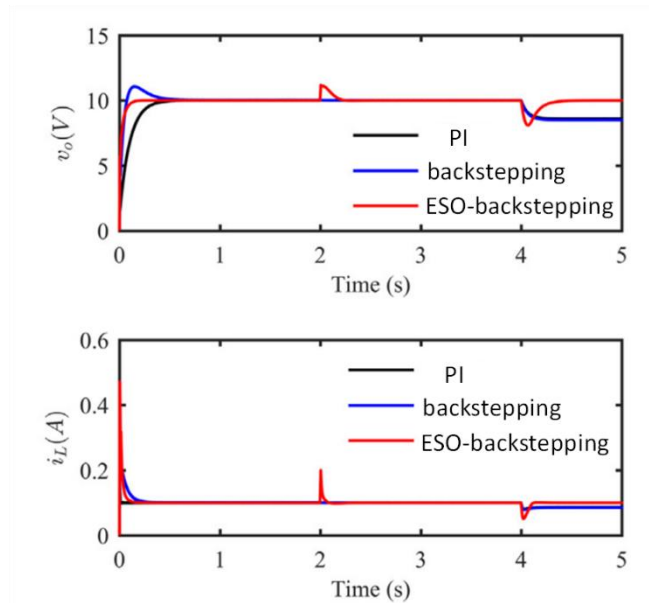


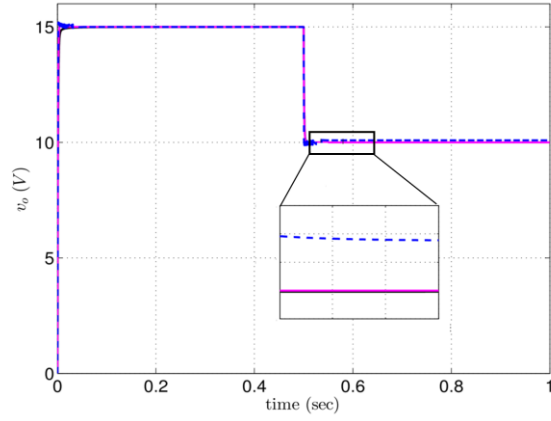
Figure 8. Buck converter with step change of input voltage

### 6.3 Case 3: Reference Voltage Variation

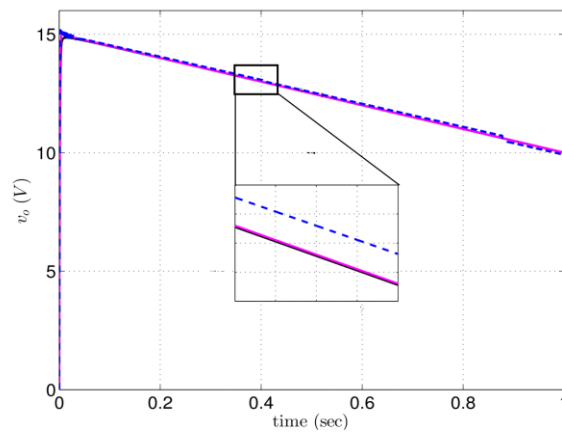
Next, the desired voltage is changed between 10 and 15 V in step, ramp, and sinusoidal form. Starting with 15V reference voltage and then it is dropped to 10V at  $t=0.5s$ . Also, ramp and sinusoidal reference voltage are changed between 15 and 10V. From the results shown in Fig. 9, it can be observed that the ESO-backstepping and backstepping could exactly track the variable voltage while it has a steady state error in the order of 0.13 V. Compared with the backstepping, the ESO-based backstepping oscillates with small magnitude and has shorter transient response.

### 6.4 Case 4: Continuous Load Resistance

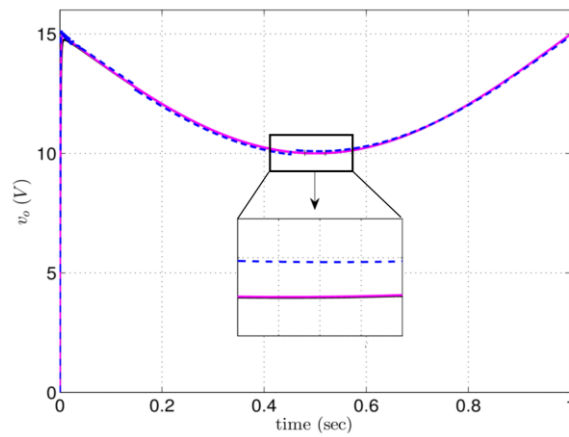
To evaluate the performance of the proposed control method with time-varying disturbance in continuous variation, the load resistor is set as  $R = 20 \sin(0.5\pi t)$ . The controller configurations remain the default value, the simulation results are given in Fig. 10. It can be seen that ESO-backstepping achieves high disturbance rejection against the continuous variation of load with faster dynamic response and zero steady-state error. However, backstepping has a 2.3% steady tracking error. The PI is insufficient to track the reference output voltage due to the high oscillation and 27% steady-state error.



(a)



(b)



(c)

Figure 9. Buck converter with step change of reference voltage (a) step (b) ramp and (c) sinusoidal

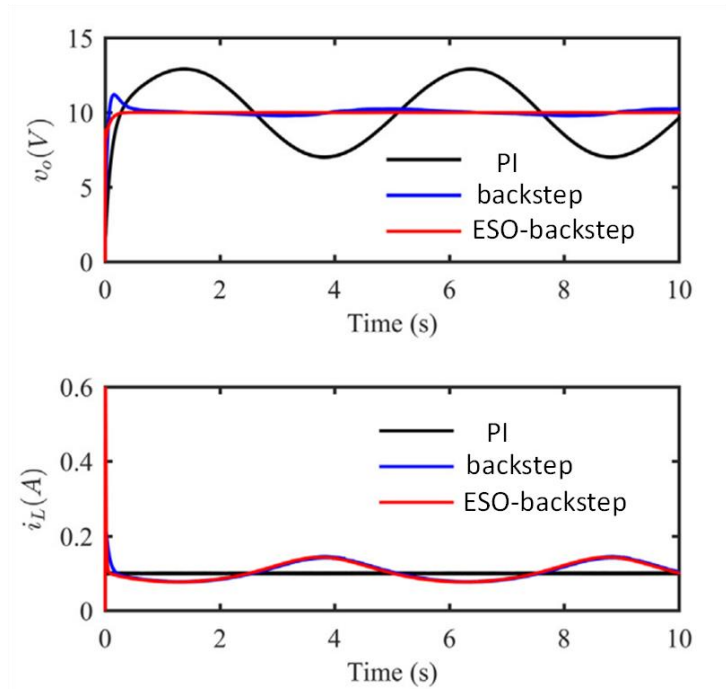


Figure 10. Buck converter with time-varying load

## 7. CONCLUSION

In this paper, an extended state observer-based backstepping control approach is implemented to a buck converter, to provide a steady DC bus voltage. The ESO-backstepping is designed for the estimation of unmatched load current. Then, a backstepping control law is consolidated with the estimated load current, which makes the robust control law. Simulation results display the performance of the proposed control scheme, with a fast transient response, zero steady-state error, and robustness against uncertainties and disturbances.

## REFERANSLAR

- [1] Dai, P., Cauet, S., & Coirault, P. (2016). Disturbance rejection of battery/ultracapacitor hybrid energy sources. *Control Engineering Practice*, 54, 166–175.
- [2] Wang, J., Li, S., Yang, J., Wu, B., & Li, Q. (2016). Finite-time disturbance observer based non-singular terminal sliding-mode control for pulse width modulation-based DCDC buck converters with mismatched load disturbances. *IET Power Electronics*, 9(9), 1995–2002.
- [3] König, O., Gregorčič, G., & Jakubek, S. (2013). Model predictive control of a DC–DC converter for battery emulation. *Control Engineering Practice*, 21(4), 428–440.
- [4] Zhong, Q.-C., & Hornik, T. (2013). *Control of power inverters in renewable energy and smart grid integration*. IEEE-Wiley Press.
- [5] Labbe, B., Allard, B., Lin-Shi, X., & Chesneau, D. (2013). An integrated sliding-mode buck converter with switching frequency control for battery-powered applications. *IEEE Transactions on Power Electronics*, 28(9), 4318–4326.

- [6] Silva-Ortigoza, R., Hernández-Guzmán, V. M., Antonio-Cruz, M., & Muñoz-Carrillo, D. (2015). DC/DC Buck power converter as a smooth starter for a DC motor based on a hierarchical control. *IEEE Transactions on Power Electronics*, 30(2), 1076–1084.
- [7] Chen, Z., Gao, W., Hu, J., & Ye, X. (2011). Closed-loop analysis and cascade control of a nonminimum phase boost converter. *IEEE Transactions on Power Electronics*, 26(4), 1237–1252.
- [8] Walker, G. R., & Sernia, P. C. (2004). Cascaded DC-DC converter connection of photovoltaic modules. *IEEE Transactions on Power Electronics*, 19(4), 1130–113.
- [9] J. Alvarez-Ramirez, G. Espinosa-Perez, and D. Noriega-Pineda, “Current- mode control of DC–DC power converters: A backstepping approach,” *Int. J. Robust Nonlinear Control*, vol. 13, no. 5, pp. 421–442, Apr. 2003.
- [10] C. Olalla, R. Leyva, A. E. Aroudi, and I. Queinnec, “Robust LQR control for PWM converters: An LMI approach,” *IEEE Trans. Ind. Electron.*, vol. 56, no. 7, pp. 2548–2558, Jul. 2009.
- [11] Q.-C. Zhong and T. Hornik, “Cascaded current–voltage control to improve the power quality for a grid-connected inverter with a local load,” *IEEE Trans. Ind. Electron.*, vol. 60, no. 4, pp. 1344–1355, Apr. 2013.
- [12] G. Escobar, A. Valdez, J. Leyva-Ramos, and P. Martínez, “A controller for a boost converter with harmonic reduction,” *IEEE Trans. Control Syst. Technol.*, vol. 12, no. 5, pp. 717–726, Sep. 2004.
- [13] G. J. Jeong, I. H. Kim, and Y. I. Son, “Design of an adaptive output feedback controller for a DC/DC boost converter subject to load variation,” *Int. J. Innov. Comput. Inf. Control*, vol. 7, no. 2, pp. 791–803, Feb. 2011.
- [14] J. Linares-Flores, A. H. Mendez, C. García-Rodríguez, and H. SiraRamírez, “Robust nonlinear adaptive control of a boost converter via algebraic parameter identification,” *IEEE Trans. Ind. Electron.*, vol. 61, no. 8, pp. 4105–4114, Aug. 2014.
- [15] E. Vidal-Idiarte, C. E. Carrejo, J. Calvente, and L. Martínez-Salamero, “Two-loop digital sliding mode control of DC–DC power converters based on predictive interpolation,” *IEEE Trans. Ind. Electron.*, vol. 58, no. 6, pp. 2491–2501, Jun. 2011.
- [16] S. Oucheriah and L. Guo, “PWM-based adaptive sliding-mode control for boost DC–DC converters,” *IEEE Trans. Ind. Electron.*, vol. 60, no. 8, pp. 3291–3294, Aug. 2013.
- [17] O. Lopez-Santos, L. Martinez-Salamero, G. Garcia, H. Valderrama-Blavi, and T. Sierra-Polanco, “Robust sliding-mode control design for a voltage regulated quadratic boost converter,” *IEEE Trans. Power Electron.*, vol. 30, no. 4, pp. 2313–2327, Apr. 2015.
- [18] L. Guo, J. Y. Hung, and R. M. Nelms, “Evaluation of DSP-based PID and fuzzy controllers for DC–DC converters,” *IEEE Trans. Ind. Electron.*, vol. 56, no. 6, pp. 2237–2248, Jun. 2009.
- [19] R.-J. Wai and L.-C. Shih, “Adaptive fuzzy-neural-network design for voltage tracking control of a DC–DC boost converter,” *IEEE Trans. Power Electron.*, vol. 27, no. 4, pp. 2104–2115, Apr. 2012.
- [20] S. E. Beid and S. Doubabi, “DSP-based implementation of fuzzy output tracking control for a boost converter,” *IEEE Trans. Ind. Electron.*, vol. 61, no. 1, pp. 196–209, Jan. 2014.
- [21] J. Linares-Flores, J. L. Barahona-Avalos, H. Sira-Ramírez, and M. A. Contreras-Ordaz, “Robust passivity-based control of a buck–boostconverter/dc-motor system: An active disturbance rejection approach,” *IEEE Trans. Ind. Appl.*, vol. 48, no. 6, pp. 2362–2371, Nov./Dec. 2012.

- [22] Y.-X. Wang, D.-H. Yu, and Y.-B. Kim, "Robust time-delay control for the DC–DC boost converter," *IEEE Trans. Ind. Electron.*, vol. 61, no. 9, pp. 4829–4837, Sep. 2014.
- [23] M. Sitbon, S. Schacham, and A. Kuperman, "Disturbance observer based voltage regulation of current-mode-boost-converter-interfaced photovoltaic generator," *IEEE Trans. Ind. Electron.*, vol. 62, no. 9, pp. 5776–5785, Sep. 2015.
- [24] Zhang, Q., Min, R., Tong, Q., Zou, X., Liu, Z., & Shen, A. (2014). Sensorless predictive current controlled DC–DC converter with a self-correction differential current observer. *IEEE Transactions on Industrial Electronics*, 61(12), 6747–6757.
- [25] Cucuzzella, M., Lazzari, R., Trip, S., Rosti, S., Sandroni, C., & Ferrara, A. (2018). Sliding mode voltage control of boost converters in DC microgrids. *Control Engineering Practice*, 73, 161–170.
- [26] S. Jiang, D. Cao, Y. Li, J. Liu, and F. Z. Peng, "Low-THD, fasttransient, and cost-effective synchronous-frame repetitive controller for three-phase UPS inverters," *IEEE Trans. Power Electron.*, vol. 27, no. 6, pp. 2994–3005, Jun. 2012.
- [27] Tan, S.-C., Lai, Y., Tse, C. K., & Cheung, M. K. (2006). Adaptive feedforward and feedback control schemes for sliding mode controlled power converters. *IEEE Transactions on Power Electronics*, 21(1), 182–192.
- [28] I. Son and I. H. Kim, "Complementary PID controller to passivity based nonlinear control of boost converters with inductor resistance," *IEEE Trans. Control Syst. Technol.*, vol. 20, no. 3, pp. 826–834, May 2012.
- [29] Kim, S.-K., & Lee, K.-B. (2015). Robust feedback-linearizing output voltage regulator for DC-DC boost converter. *IEEE Transactions on Industrial Electronics*, 62(11), 7127–7135.
- [30] H. K. Khalil, *Nonlinear Systems*. Englewood Cliffs, NJ, USA: PrenticeHall, 2002.
- [31] J. Alvarez-Ramirez, G. Espinosa-Perez, and D. Noriega-Pineda, "Current- mode control of DC–DC power converters: A backstepping approach," *Int. J. Robust Nonlinear Control*, vol. 13, no. 5, pp. 421–442, Apr. 2003.
- [32] Huang, A.-C., & Chen, Y.-C. (2004). Adaptive multiple-surface sliding control for nonautonomous systems with mismatched uncertainties. *Automatica*, 40(11), 19.
- [33] Choi, H. H. (2007). LMI-based sliding surface design for integral sliding mode control of mismatched uncertain systems. *IEEE Transactions on Automatic Control*, 52(4), 736–742.
- [34] J. Han, "From PID to active disturbance rejection control," *IEEE Trans. Ind. Electron.*, vol. 56, no. 3, pp. 900–906, Mar. 2009.